PRESSURE MEASUREMENTS FOR
TRANSLATING HYDROSTATIC THRUST BEARINGS

Aaron B. Crabtree [1], Noah D. Manring [1] and Robert E. Johnson [2]

[1] *Mechanical and Aerospace Engineering Department University of Missouri – Columbia, Columbia, MO 65211*
[2] *The William States Lee College of Engineering University of North Carolina – Charlotte, Charlotte, NC 28223*

Abstract

The objective of this study is to take insitu measurement of the pressure profile that exists between a sliding thrust bearing and a stationary thrust surface. Using a two-dimensional model of the bearing and the classical one-dimensional Reynolds equation, the experimental results are explained and the minimum fluid film thickness and the tilt angle of the bearing are numerically determined. In this work, it is shown that the bearings tilt into the leading edge of the bearing and that the minimum fluid-film thickness at the leading edge of the bearing is on the order of the surface roughness. This work provides fundamental insight into the problem of metal-to-metal contact for thrust bearings.

1 Introduction

1.1 Background

Hydrostatic thrust bearings are commonly used in hydraulic pumps and motors. These bearings are particularly used for slow speed operation while supporting large loads. The bearings are designed with a large deep pocket where pressurized fluid is injected. This pressurized fluid lifts the bearing off the thrust surface to obtain a desired fluid film under the sealing lands of the bearing. This fluid film gap separates the two surfaces thus preventing metal-to-metal contact. Hydrostatic bearings are very sensitive to manufacturing tolerances and operating conditions, which makes them prone to sudden and catastrophic failures. Therefore, there exists an ongoing need to understand the driving factors that cause hydrostatic bearings to fail. This work is put forward to enhance the understanding of these bearings as they operate within hydraulic pumps and motors.

1.2 Literature Review

There are numerous papers and books on the topic of hydrostatic thrust bearings and only a brief review of the relevant literature will be discussed here. Kazama and Yamauchi (1993) studied the effect of the physical and geometric properties of hydrostatic thrust bearings on the power loss, load carrying capacity, and moment stiffness. Their analysis determined that the pocket radius, orifice size and length, and sealing land width had direct effects on the bearings operations and gave optimum design parameters for these variables. They also discussed the effect of cyclic pressure and eccentric loading on the fluid film thickness. Koc and Hooke (1992, 1996) discussed the effects of the clamping ratio on the fluid film and the tilting moments. In this work, it was also discovered that when one introduces an orifice into the bearing pocket, the bearing response becomes unstable. It was also shown that the film thickness has an inverse relationship to the orifice size. Iboshi and Yamaguchi (1982, 1983) analytically determined the equation of motion of the thrust bearing and found that the speed and pump pressure have a direct impact on the fluid film thickness. Manring (2001) investigated the dynamic characteristics of thrust bearing tipping within an axial-piston pump. In this work, the driving factors relating bearing tipping with reciprocating and centrifugal inertia of the slipper/piston assembly were identified. Other work by Manring et al (2002, 2004) has been aimed at understanding the impact of bearing deformations on the load-carrying capacity and flow rate of stationary bearings.

The various authors just mentioned have analytically or experimentally described various characteristics of the hydrostatic thrust bearing using restricted assumptions or imposed operational constraints. Howev-

er, none of this work has been carried out using insitu measurements of the pressure profile between a sliding bearing and a stationary thrust surface during typical operating speeds and pressures (7 to 42-MPa) of the machine. This present work is intended to augment the body of literature by providing these measurements with analytical explanations for the results.

1.3 Objective

The objective of this study is to take insitu measurement of the pressure profile that exists between a sliding thrust bearing and a stationary thrust surface. Using a two-dimensional model of the bearing and the classical one-dimensional Reynolds equation, the experimental results are explained and the minimum fluid film thickness and the tilt angle of the bearing are numerically determined. In this work, it is shown that the bearings tilt into the leading edge of the bearing and that the minimum fluid-film thickness at the leading edge of the bearing is on the order of the surface roughness. This work provides fundamental insight into the problem of metal-to-metal contact for thrust bearings.

2 Experiments

A schematic of the thrust bearing test stand is shown in Fig. 1. The test stand was designed to simulate the actual environment of a bearing application within a hydraulic pump. As shown in Fig. 1, the piston/bearing assembly was mounted within a cylinder block that was rotated about a centerline axis at an angular velocity ω. Though it is not shown in Fig. 1, three piston/bearing assemblies were used within the cylinder block for the purposes of balancing the system. The three piston/bearing assemblies were evenly spaced at 120° increments and were located a distance r away from the centerline of the cylinder block ($r = 75$ mm). By rotating the cylinder block (as is done within an actual hydraulic pump), the bearings were forced to slide relative to the thrust surface at a velocity given by $r \cdot \omega$. Figure 1 shows a lubrication level that is higher than the piston/bearing ball joint. This condition ensured that the bearing was fully submerged in lubricant during the experiments, which also simulates an actual pump environment. A pressure compensated pump supplied pressurized fluid to the cylinder block through a manifold system within the test stand structure. The cylinder block was rotated by an AC motor equipped with a variable frequency drive. As shown in Fig. 1, pressure sensors were positioned in the thrust surface near the centerline of the bearing path. As the bearings passed over the pressure sensors, high frequency insitu pressure measurements were taken and recorded. Pressure measurements were accurate with 1.5% of their maximum measured values.

Figure 2 shows a representative plot of pressure data taken for a cylinder block rotational speed of 150 rpm. In this figure, the pressure profile across the leading land is shown to the left while the pressure profile across the trailing land is shown to the right. The middle zone of this figure describes the measured pressure

within the bearing pocket, which is approximately equal to the supply pressure of the test rig. The physical geometry of the bearing is shown in Fig. 2 by the dimensions s and L (11.25-mm and 16.5-mm respectively). As shown in Fig. 2, the pressure on the leading land is nearly non-existent until the very edge of the pocket is reached. This is much different as compared to the trailing land where pressure is maintained across a healthy portion of the sealing land. The differences in the pressure distribution across the two lands may be explained by lubrication analysis that follows.
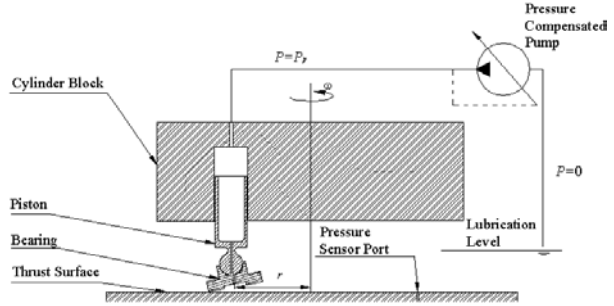

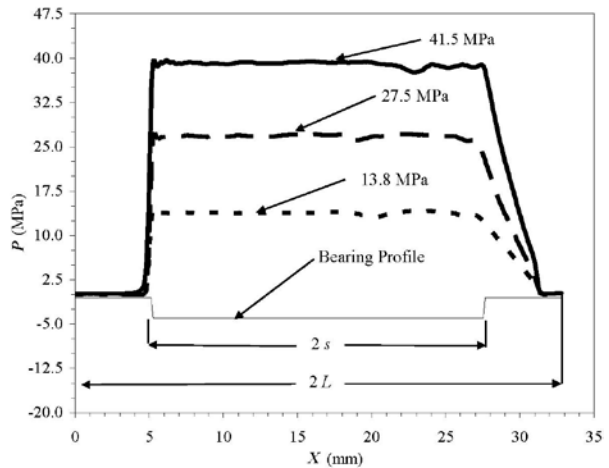**Fig. 1:** *Hydrostatic thrust bearing operation*

Fig. 2: *Pressure profile under a hydrostatic thrust bearing at 150 RPM*

3 Analysis

3.1 Dimensionless Variables

The analysis of the pressure profile between the bearing and the thrust surface will be carried out using dimensionless equations. To conduct this analysis, the following dimensionless variables will be used:

$$\hat{P} = \frac{P}{P_0}, \quad \hat{Q} = \frac{Q}{\dfrac{\overline{h}^3 P_0}{6\mu L}}, \quad \hat{U} = \frac{U}{\dfrac{\overline{h}^2 P_0}{6\mu L}},$$

$$\hat{h} = \frac{h}{\overline{h}}, \quad \hat{x} = \frac{x}{L}, \quad \hat{s} = \frac{s}{L}, \tag{1}$$

where the definition of each symbol is given in the Nomenclature section of this paper. Note: the symbols with carets are dimensionless while all other symbols have dimensions.

3.2 Bearing Description

Figure 3 shows the geometry of the bearing to be studied in this section of the paper. The bearing is separated by an average fluid film gap, $\bar{h}$, with the maximum and minimum thickness at the bearing edges, depending on the sign of the tilt angle, θ. The pocket is assumed to be significantly deep compared to the fluid film and has a radius, s. This deep pocket provided a constant pressure profile approximately equal to the supply pressure. The bearing has an outside radius, L, and has a relative velocity, U, to the thrust surface.
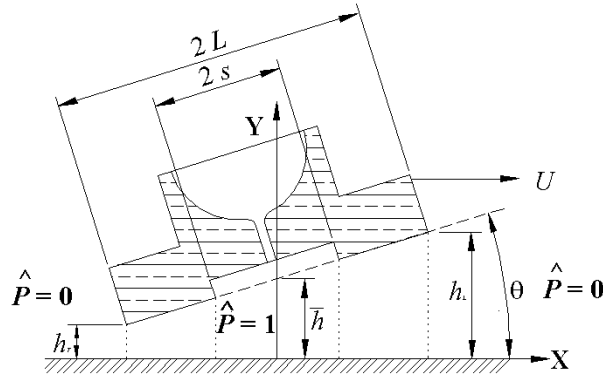

Fig. 3: *Hydrostatic thrust bearing geometry*

3.3 Governing Equation

The fluid flow within the gap of the sealing land and the thrust surface is assumed a low Reynolds number flow. Thus, using the two-dimensional rectangular coordinates shown in Fig. 3, the classic lubrication equation that defines the fluid pressure between the two surfaces along the bearings centerline path is given by:

$$\frac{d\hat{P}}{d\hat{x}} = -\left\{ \frac{2\hat{Q}}{\hat{h}^3} + \frac{\hat{U}}{\hat{h}^2} \right\}, \tag{2}$$

where $\hat{x}$ is the linear distance from the center of the bearing in the direction of motion, $\hat{Q}$ is the volumetric flow rate across a bearing land, $\hat{h}$ is the fluid film gap which varies linearly with the dimension, $\hat{x}$ and $\hat{U}$ are the relative velocity of the bearing. A derivation for this equation is provided in previous literature (Manring, 2005). Equation 2 assumes that the pressure does not vary in the y-direction and that the fluid flow is relatively constant along the centerline path. One may note that Eq. 2 is the governing equation for an infinite plain bearing, which is acceptable for this analysis due to the significantly small film thicknesses that typicaly occur compared to the very large plate width in these bearings types (tens of micrometers compared to tens of millimeters). In Fig. 3, the thrust bearing geometric boundaries and the boundary pressure conditions are given by:

$$\hat{P}(\pm 1) = 0,$$
$$\hat{P}(-\hat{s} \le \hat{x} \le \hat{s}) = 1, \tag{3}$$

where the pressure under the pocket is assumed constant and equal to the pump pressure and the tank pres-

sure is vented to atmosphere. These boundary conditions, when applied to Eq. 2, provide two separate differential equations that describe the pressure profiles corresponding to the leading and trailing lands.

3.4 Fluid Film Description

The average fluid film thickness is shown in Fig. 3 by the symbol $\bar{h}$. Using Fig. 3, this dimension is given by:

$$\bar{h} = \frac{1}{2}(h_{\mathrm{L}} + h_{\mathrm{T}}), \tag{4}$$

where h_{L} and h_{T} is the height of the leading and trailing lands at the bearing edges. Due to the small tilt angle of the bearing and neglecting bearing deflection for now, the fluid film across both sealing lands may be described as:

$$h = \bar{h} + \theta x, \tag{5}$$

where θ is the tilt angle of the bearing. Substituting the dimensionless variables into Eq. 5 we obtain:

$$\hat{h} = 1 + \alpha \hat{x}, \tag{6}$$

where α is the coefficient of tilt given by:

$$\alpha = \frac{L}{h}\theta, \tag{7}$$

This parameter will be numerically determined in this study using the lubrication theory and the pressure measurements.

3.5 Pressure Profile Solution

Substituting Eq. 6 into Eq. 2 and performing a single integration with the prescribed boundary conditions, the pressure profile under the thrust bearing lands may be determined. These results are given by:

$$\hat{P}_{\mathrm{L}}(\hat{x}) = \frac{(1-\hat{x})(1+\hat{s}\alpha)^2(2+\alpha+\hat{x}\alpha)}{(1-\hat{s})(1+\hat{x}\alpha)^2(2+\alpha+\hat{s}\alpha)}$$
$$+\hat{U}\left(\frac{(\hat{x}+\hat{s})(1-\hat{x})\alpha}{(1+\hat{x}\alpha)^2(2-\alpha-\hat{s}\alpha)}\right), \quad \hat{s} \le \hat{x} \le 1, \tag{8}$$

$$\hat{P}_{\mathrm{T}}(\hat{x}) = \frac{(1+\hat{x})(\hat{s}\alpha-1)^2(2-\alpha+\hat{x}\alpha)}{(1-\hat{s})(1+\hat{x}\alpha)^2(2-\alpha-\hat{s}\alpha)}$$
$$-\hat{U}\left(\frac{(\hat{x}+\hat{s})(1+\hat{x})\alpha}{(1+\hat{x}\alpha)^2(2-\alpha-\hat{s}\alpha)}\right), \quad -1 \le \hat{x} \le \hat{s}, \tag{9}$$

where $\hat{P}_{\mathrm{L}}$ is the pressure beneath the leading land and $\hat{P}_{\mathrm{T}}$ is the pressure beneath the trailing land. These solutions show that the pressure profile is dependent on the pocket radius $\hat{s}$, the coefficient of tilt α, and relative velocity of the bearing $\hat{U}$. Equations 8 and 9 are shown in two parts; the first describes the hydrostatic effect of the bearing and the second describes the hydrodynamic effects.

4 Numerical Correlation

Equations 8 and 9 are two independent equations that describe the pressure profile underneath the leading and trailing lands respectively. In this study, the pressure on the left-hand-side of these equations has been measured for a given bearing geometry with a pocket radius given by $\hat{s}$. The remaining unknown variables in these two equations are given by the coefficient of tilt α and the dimensionless sliding velocity $\hat{U}$. By selecting pressure measurements from each land, Eq. 8 and 9 may be simultaneously solved for α and $\hat{U}$ using a Newton-Raphson method. Once these parameters have been determined the average fluid film thickness may be extracted from $\hat{U}$, assuming that we know the fluid viscosity. The bearing tilt angle may then be extracted from α. These extractions provide quantified results for the minimum fluid-film thickness and the bearing tilt.

5 Results and Discussion

Using the above numerical approach, it has been determined from this study that $\alpha = -0.598$ and $\hat{U} = 80.0$ for the data presented in Fig. 2 with $\mu = 0.02$ -Ns/m^2. These results correspond to a tilt angle that is given by $\theta = -0.00172°$ and a minimum fluid film thickness at the leading edge of the bearing given by $h_L = 0.331$ -μm. Note: the surface roughness is on this order which means that metal-to-metal contact at the leading edge is likely to occur. Using the numerically determined values for α and $\hat{U}$, Eq. 8 and 9 are plotted in Fig. 4 and 5 along with the experimental pressure results. The experimental results were converted into non-dimensional units based upon Eq. 1.

Figure 4 shows the pressure profile beneath the leading land for experimental results taken at three different pressures. A quantitative result is also plotted in this figure based upon Eq. 8; however, in the region where this equation predicts a negative pressure the result has been set to zero. In other words, the analysis presented in Eq. 8 is only valid as long is it predicts a positive pressure. Using the dimensionless parameters of $\alpha = -0.598$ and $\hat{U} = 80.0$, Eq. 8 will predict a negative pressure beneath the leading land for $1 > \hat{x} > 0.71$. This analytical result suggests that under this portion of the land fluid is either vaporizing under extremely low pressures, or fluid is backfilling from the sides of the bearing to make up for fluid that is lost at the no-slip boundary surface due to sliding and the direction of bearing tilt. Equation 8 is not able to predict either of these cases and is therefore truncated when the results become unreasonable. It should be noted, however, that where pressures are positive Eq. 8 does a very nice job of matching the experimental results that are shown in Fig. 4. Without changing the values of α and $\hat{U}$ it will be shown in the next figure that Eq. 9 produces similarly adequate results for the trailing land.
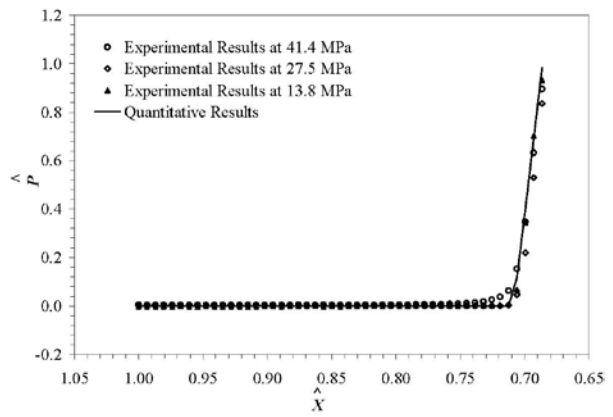

Fig.4: *Pressure profile under leading land of bearing at 150 RPM*

Figure 5 shows the pressure profile beneath the trailing land for experimental results taken at three different pressures. A quantitative result is also plotted in this figure based upon Eq. 9. In this result, no truncations of Eq. 9 were required as all predicted pressures were positive and no unrealistic results were produced by the analysis. Again, the quantitative results of Fig. 5 were produced for $\alpha = -0.598$ and $\hat{U} = 80.0$, which were the same values used for the analysis of the leading land. Figure 5 shows good correlation between the experiments and the analysis for $\hat{x} > -0.89$. As shown in this figure, the experiments indicated a sudden change in pressure near $\hat{x} = -0.89$, which cannot be explained beyond doubt in this present work. A possible solution may be found in the deformation of the bearing which results from the cantilevered condition of the land relative to the structure of the ball-and-sockt joint. The analysis of Eq. 9 will not predict this effect as it assumes a perfectly flat bearing in a tilted condition.
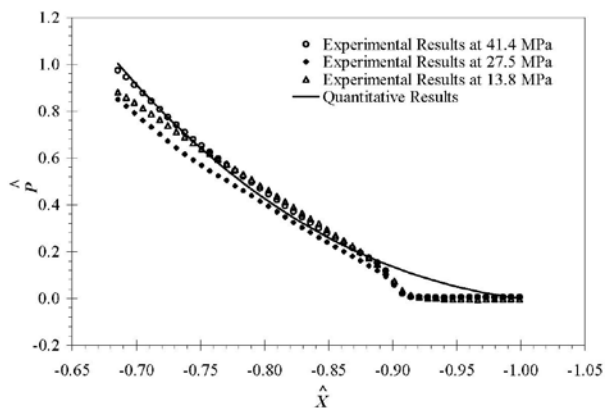

Fig. 5: *Pressure profile under trailing land of bearing at 150 RPM*

A difference between the pressure results of the leading and trailing lands has been shown in Fig. 4 and 5. The analysis of Eq. 8 and 9 lends insight into these differences by describing both hydrostatic and hydrodynamic effects within the results. The hydrostatic effects are described in the first term of these equations while the hydrodynamic effects are described in the second term of these equations. In short, due to the tilt-

ed direction of the bearing as shown by a negative value for α, the pressure reducing hydrodynamic effects are smaller for the trailing land as opposed to the leading land. In other words, the sliding effects are the cause of these differences and the analysis predicts the observed phenomenon. These pressure differences produce a tilting moment on the bearing which tends to enhance the direction of tilt, causing the bearing to "dig" into the thrust surface. For this reason, metal-to-metal contact is commonly observed with machines that use hydrostatic thrust bearings.

6 Conclusion

The following conclusions are supported by the results of this research:

The lubrication mechanism between the hydrostatic thrust bearing and the thrust surface can be reasonably modeled using the one dimensional Reynolds equation. These results are presented in Eq. 8 and 9 for a tilted bearing undergoing translation.

Using the lubrication models presented in Eq. 8 and 9 and actual pressure measurements, the tilt angle and minimum fluid film thickness between the bearing and the thrust surface may be inferred using the numerical approach described in this paper. In other words, proximity sensors are not needed to obtain these results.

The pressures beneath the leading and trailing seal lands of the hydrostatic thrust bearing are significantly different due to the angular tilt of the bearing.

The angular tilt of the bearing causes the leading edge to tilt into the thrust surface, thus creating a minimum fluid-film thickness at the leading edge.

The minimum fluid film thickness between the bearing and the thrust surface is on the order of the surface roughness. Therefore, metal-to-metal contact is expected at this interface, which explains the contact patterns that have been observed in the test device and in practice.

Nomenclature

h	fluid film thickness between the bearing and thrust surface
h_L	fluid film at the outside the leading land of the thrust bearing
h_T	fluid film at the outside the trailing land of the thrust bearing
$\bar{h}$	average fluid film thickness
L	outer radius of the bearing
P	fluid pressure between the bearing and thrust surface
P_L	fluid pressure under the leading land of the thrust bearing
P_T	fluid pressure under the trailing land of the thrust bearing
P_0	pocket pressure
Q	fluid flow rate passing under the trailing or leading lands
r	distance from the piston block centerline to

	the sensor location on the thrust bearing
s	pocket radius of the thrust bearing
U	translating velocity of the thrust bearing
x	primary rectangular coordinate
α	coefficient of bearing tilt
μ	fluid absolute viscosity
θ	bearing tilt angle
ω	angular velocity

Acknowledgements

References

Iboshi, N. and **Yamaguchi, A.** 1982, "Characteristics of a Slipper Bearing for Swash Plate Type Axial Piston Pumps and Motors (1st Report, Theoretical Analysis)," *Bulletin of the JSME*, Vol. 25 No. 210, pp. 1921-1930.

Iboshi, N. and **Yamaguchi, A.** 1983, "Characteristics of a Slipper Bearing for Swash Plate Type Axial Piston Pumps and Motors (2nd Report, Experiment)," *Bulletin of the JSME*, Vol. 26 No. 219, pp. 1583-1589.

Kazama, T. and **Yamaguchi, A.** 1993, "Optimum Design of Bearing and Seal Parts for Hydraulic Equipment," *Wear*, Vol. 161, pp. 161-171.

Koc, E. and **Hooke, C. J.** 1992, "Slipper Balance in Axial Piston Pumps and Motors," *ASME Journal of Tribology*, Vol. 114, pp. 766-772.

Koc, E. and **Hooke, C. J.** 1996, "Investigation into the Effects of Orifice Size, Offset and Overclamp Ratio on the Lubrication of Slipper Bearings," *Tribology International*, Vol. 29 No. 4, pp. 299-305.

Manring, N. D. 2001. Predicting the required slipper hold-down force within an axial-piston swash-plate type hydrostatic pump. *ASME International Mechanical Engineering Congress and Exposition*. New York, NY.

Manring, N.D. 2005. *Hydraulic Control Systems*. John Wiley & Sons. Holboken, New Jersey

Manring, N. D., **Johnson, R. E.**, and **Cherukuri, H..** 2002. The impact of linear deformations on stationary hydrostatic thrust bearings. *ASME Journal of Tribology*, Technical Brief. 124:874-77.

Manring, N. D., **Wray, C. L.**, and **Dong, Z..** 2004. Experimental studies on the performance of slipper bearings within axial-piston pumps. *ASME Journal of Tribology*. 126:511-18.

Aaron B. Crabtree
Born 1977, he was raised on a small family farm outside Odessa, Missouri, USA. Aaron received his B.S. in Agricultural Engineering and Mechanical Engineering in 2000, and his M.S. in Mechanical Engineering in 2003, all three from the University of Missouri – Columbia. His research interests are in off-highway machine & component test, sensor development, and hydraulic system & component development. He is currently a Ph.D. candidate at the University of Missouri - Columbia.

Noah D. Manring
Born 1967 in Del Norte, Colorado, USA. Dr. Manring received his B.S. and B.A. degrees from Michigan State University, his M.S. degree from the University of Illinois at Urbana-Champaign, and his Ph.D. degree from Iowa State University. Dr. Manring is currently the James C. Dowell Professor of Mechanical Engineering at the University of Missouri - Columbia (UMC). Before joining the faculty at UMC, he worked for eight years in the off-highway mobile equipment industry. He holds ten US patents for innovations in the field of fluid power. As a professor, he has received research funding from Caterpillar, Inc., Festo Corp., and the National Fluid Power Association, among others, as well as the US Department of Education, the National Science Foundation, and various private donors. Dr. Manring currently serves as an associate editor of the International Journal of Fluid Power and the Journal of Dynamic Systems, Measurement and Control. He has done consulting work for several industrial firms including Moog Inc., FMC Wyoming Corp., Dennison Hydraulics, and Parker Hannifin. Dr. Manring is the recent author on a new textbook entitled, Hydraulic Control Systems, published by John Wiley & Sons.

Robert E. Johnson
Dr. Johnson is originally from Hicksville, NY, received his B.S. degree from SUNY at Buffalo, and his M.S. and Ph.D. degrees from Caltech. Dr. Johnson is currently Dean of The William States Lee College of Engineering at The University of North Carolina at Charlotte. Before joining the faculty at UNC Charlotte, he worked for sixteen years in the Department of Theoretical and Applied Mechanics at the University of Illinois. He works in the area of fluid mechanics, material processing, metal forming, race car aerodynamics and asymptotic methods. He is the author or coauthor on more that 70 archival journal articles, and has worked on numerous projects for the National Science Foundation, Alcoa and Caterpillar. Dr. Johnson serves on the Board of Governors for NC Polymer Center of Excellence and on the Board of Advisors for the Ben Craig Center, a business incubator in Charlotte.